Modelling of monopile response to cyclic lateral loading in sand

C N Abadie, Byron Byrne, Guy Houlsby

MODELLING OF MONOPILE RESPONSE TO CYCLIC LATERAL LOADING IN SAND

C.N. Abadie, B.W. Byrne & G.T. Houlsby
Department of Engineering Science, University of Oxford

Abstract
This paper outlines experimental and theoretical research exploring the response of rigid piles to cyclic lateral loading, relevant to large diameter monopiles for offshore wind applications. The experimental work comprised of 1-g laboratory scale model tests in sand, where up to 100,000 cycles were applied. The tests were designed specifically for identification of key mechanisms behind the pile response with the results demonstrating that the resulting moment-rotation curves are dominated by ratcheting, whilst also conforming approximately to the extended Masing rules. These results provide impetus for the development of a new constitutive model, HARM, which can accurately capture the pile response to cyclic lateral loading. A brief overview of the model is presented, along with a calibration method and illustrative results. This modelling approach could, in future, be developed further to supplement current design methods for SLS and FLS.

1. Introduction

Offshore wind turbines are large structures, for which the foundation is critical and costly. The most common foundation is the monopile, which is a single stiff tubular pile of up to 8m diameter and perhaps 45m long. During their lifetime, monopiles are exposed to a range of loads of very many cycles. Because of an inadequate understanding of the effects of these loading conditions (*e.g.* DNV, 2014), currently installed monopiles may be over-designed (Kallehave *et al.*, 2012), causing excessive manufacturing, transportation and installation costs. While significant progress has been achieved on the design of monopiles for ultimate capacity (Byrne *et al.*, 2015), understanding and modelling the effects of cyclic loading is still developing. It is nonetheless recognized that, as the monopiles are made shorter and with smaller diameters, following optimization, cyclic loading could cause progressive tilting of the foundation along with changes to stiffness, damping and capacity.

This paper outlines experimental and theoretical research, aimed at providing further insight, and a new modelling technique (HARM - "Hyperplastic Accelerated Ratcheting Model") for piles in sand subjected to lateral cyclic loading. The experimental work highlights the important effects that need to be accounted for in detailed modelling. The theoretical development then elaborates on these key findings and leads to a constitutive framework that describes the soil-pile interaction response in a rigorous and concise manner. The final part of this paper demonstrates how the experimental results are used as source data for calibration of the model and demonstrates the suitability of the methodology for complex load scenarios with large cycle number.

2. Model test experiments

2.1 Background and motivation

Pile response to lateral loading is commonly assessed using the so-called *p-y* method (API, 2010, DNV, 2014). The soil-pile interaction is represented by a series of independent springs down the pile:

$$p = Ap_u \tanh\left(\frac{K_0 y}{Ap_u}\right) = E_{py,0}(x, y)\cdot y \qquad (1)$$

Where p is the local soil reaction at a specific depth x and y is the corresponding pile deflection. A is an empirical parameter, p_u is the ultimate lateral pile resistance and K_0 is the initial soil reaction.

When considering the case of cyclic loading, it is recommended (API, 2010, DNV, 2014) to reduce the parameter A to a constant value (A=0.9 for sands). This simple method was originally derived from investigation on long slender piles used in the

oil and gas industry (O'Neill and Murchison, 1983) for jacket structures, for which down-rating the ultimate lateral capacity, following cyclic loading, is appropriate. It is questionable whether this approach, which provides the same predicted response irrespective of the number of cycles applied, is relevant to offshore wind monopiles. Accordingly, alternative approaches have been proposed recently in the literature, often making use of small-scale experimental tests. The pile deflection at peak load is measured and a direct fitting of the results provides an empirical relationship between pile deflection and cycle number (e.g. LeBlanc *et al.*, 2010b, Peralta, 2010, Klinkvort, 2012).

These laws can be applied to the monotonic response (*e.g.* LeBlanc *et al.*, 2010b), or can be integrated within Equation 1 to "degrade" the monotonic *p-y* modulus with cycle number:

$$E_{py,N} = E_{py,0} N^{-\delta} \tag{2}$$

δ is an empirical parameter directly derived from the fitted empirical law (Abadie, 2015).

Despite providing a fast methodology for estimating the cyclic pile deflection, these semi-empirical models lack rigorous description of the fundamental behaviour of the soil-pile response. They do not account for change in capacity, damping or stiffness, and indeed could be misleading for the latter, as they predict a degraded soil modulus, while increased foundation stiffness has been observed (*e.g.* LeBlanc *et al.*, 2010b, Klinkvort, 2012, Abadie and Byrne, 2014). Finally, they are difficult to adapt for load packets at different amplitudes and, to do so, requires strong assumptions such as linear cumulative damage (Miner, 1945) (*e.g.* LeBlanc *et al.*, 2010a). To address this issue, an experimental investigation was performed, analysing qualitatively the key mechanisms driving the global pile response.

2.2 Experimental techniques

The experimental tests were performed using a rig developed by Rovere (2004), of which the set-up is fully described in Abadie (2015). It involved a small rigid pile, of 77mm diameter and 360mm length. A thorough consideration of scaling, applicable to this set of tests, including pile dimensions and stress level, is described in LeBlanc *et al.* (2010b), Abadie (2015) and Abadie *et al.* (2017). The load was applied at an appropriate eccentricity above ground level using a suspended mass system and a driving motor of frequency 0.106Hz (Figure 1). The pile was driven into loose dry Yellow Leighton Buzzard sand samples.

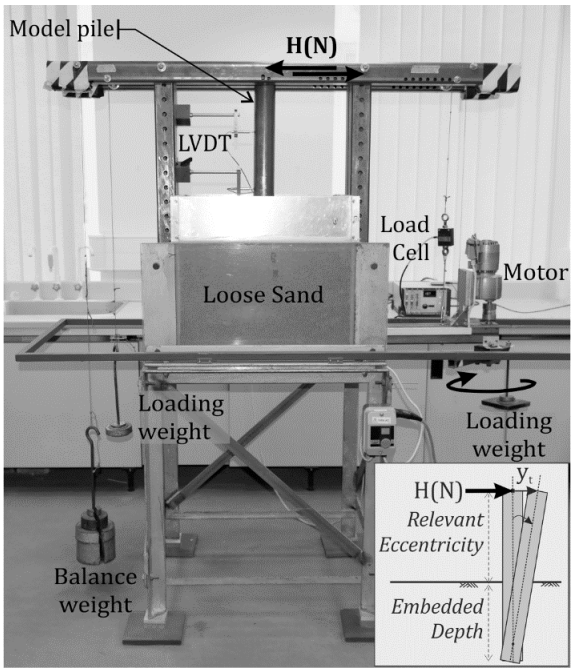

Figure 1: Lateral loading test equipment

A load cell and a pair of LVDTs enabled accurate recording of the macro-response of the pile. In the following, the test results are shown as lateral load (H) vs. displacement at the point of load application (y_t), as defined in Figure 1. For comparison with larger scale piles, both parameters are normalised using the corresponding values at ultimate capacity, designated by the subscript R and established in Abadie (2015). For consistency with Section 3, the load ratio is called σ and the displacement ratio ε:

$$\sigma = \frac{H}{H_R} \tag{3}$$

$$\varepsilon = \frac{y_t}{y_{tR}} \tag{4}$$

The tests are described in Table 1, with the load scenarios specified in terms of number of cycles N, maximum load magnitude ζ_b and amplitude ζ_c:

$$\zeta_b = \frac{H_{\max}}{H_R} = \sigma_{\max} \tag{5}$$

$$\zeta_c = \frac{H_{\min}}{H_{\max}} = \frac{\sigma_{\min}}{\sigma_{\max}} \tag{6}$$

Even though ζ_c is not zero, it is sufficiently low that the cyclic tests are considered as 1-way loading.

2.3 Monotonic response

The initial monotonic response, called the backbone curve, is observed through a simple load-reversal test (H0). The test result (Figure 2(a)) proves a hysteresis loop that conforms closely to the Masing rules (Masing, 1926): the reversed loading (unload

Table 1: Test programme

Monotonic			
H0	Symmetric reversed loading, 1.5 cycle		
HIM	Symmetric reversed loading at increasing magnitudes, 4.5 cycles (ζ_b= .31→0.44→0.56→0.69)		
Continuous cyclic			
	ζ_b	ζ_c	N
CMLT1	0.31	0.24	100, 000
CMLT2*	0.42	0.18	100, 000
CMLT3	0.47	0.13	100, 000
Continuous cyclic + Monotonic reload (* Includes CMLT2)			
CMC0	-	-	0
CMC1	0.42	0.18	1
CMC2	0.42	0.18	10
CMC3	0.42	0.18	100
CMC4	0.42	0.18	1000
CMC5	0.42	0.18	10000
Load packets of various magnitudes			
	Load History	Load Cases	
MASL1	1000×*A* - 100×*C* - 1×*E*	A: (ζ_b=0.30; ζ_c=0.11)	
MASL2	100×*C* - 1×*E* - 1000×*A*	C: (ζ_b=0.48; ζ_c=0.00)	
MASL3	1×*E* - 100×*C* - 1000×*A*	E: (ζ_b=0.69; ζ_c=0.00)	

path), scaled down by a factor of two and plotted from the origin, should match the initial loading response. This is shown by the curve "Applied Masing Rule". The graph also illustrates that the loop almost closes on reloading to the maximum past load, with negligible accumulated deformation of the pile during symmetric load reversal.

Extending this, the test denoted HIM explores the influence of increasing load magnitudes. The results (Figure 2(b)) demonstrate that the response conforms to the extended Masing rules (Pyke, 1979): (i) when exceeding the maximum load, the unloading or reloading curve follows that of the backbone curve and (ii) each time an unloading or reloading path intersects a curve from a previous cycle, the stress-stain response follows that curve.

2.4 Continuous cyclic loading

This is extended to long-term cyclic loading at non-zero mean load, for which a typical response is displayed in Figure 3 (test CMLT3). The graph shows accumulation of permanent deformation with cycle number that, despite reducing, does not decay to zero. This phenomenon is called ratcheting.

The graph also shows a tightening of the hysteresis loop during cycling, with an increase in stiffness and decrease in loop area. This effect was quantified by Abadie (2015) and Abadie *et al.*, (2017), and is of

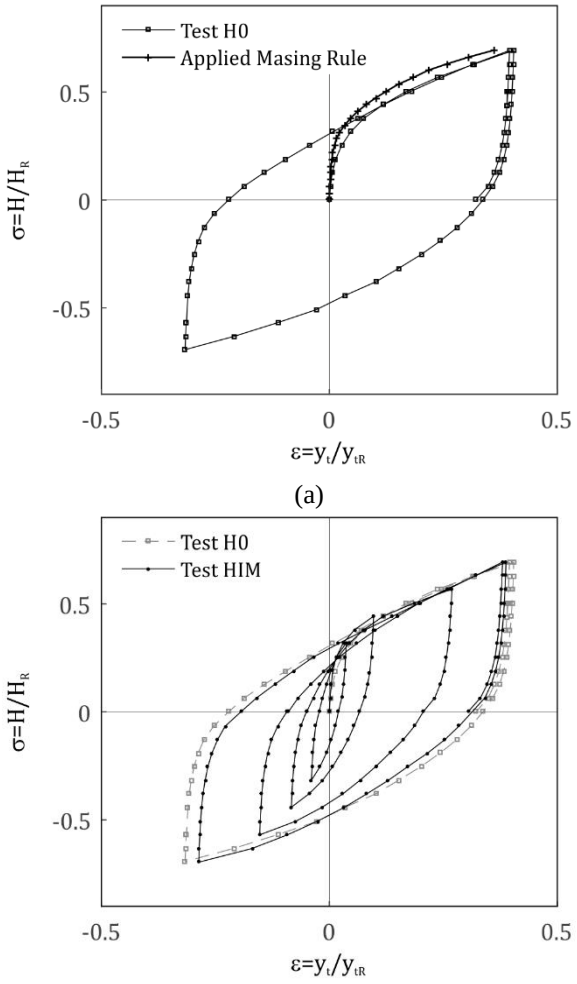

Figure 2: Test H0 and HIM: Conformation of the response to (a) the Masing Rules (Masing, 1926) and (b) the extended Masing rules (Pyke, 1979)

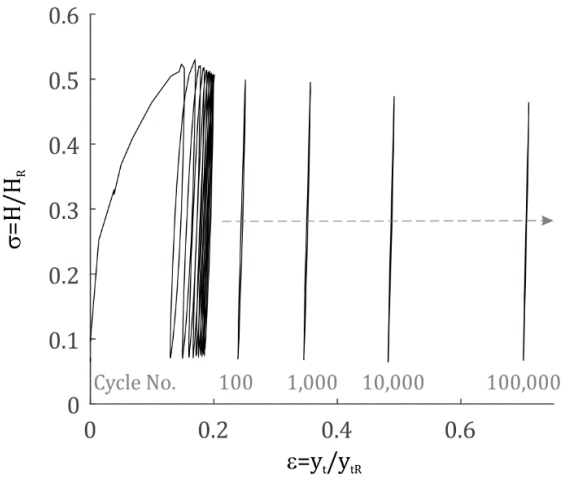

Figure 3: Test CMLT3: Load-deflection curve

second order compared to ratcheting. For instance, the secant stiffness typically increases by only 15% between 100 and 10,000 cycles.

Although the tests were performed in loose dry sand, for which larger ratcheting deformation might be expected, the underlying response of Figure 3 is in good agreement with other test results from the literature, performed at higher relative densities and

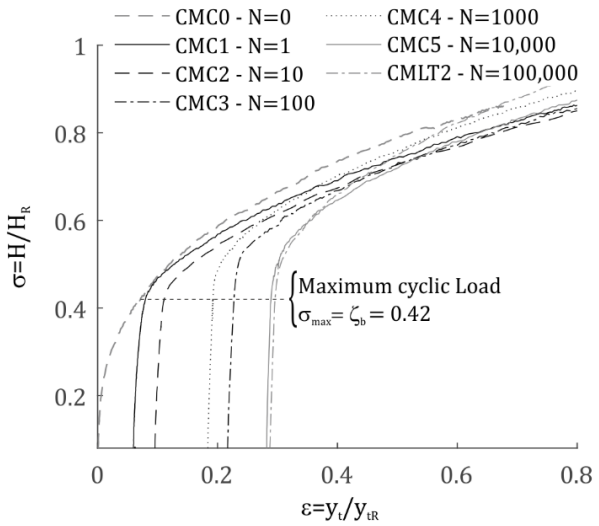

Figure 4: Tests CMC0-5, CMLT2: Reload response following cyclic loading at different cycle number

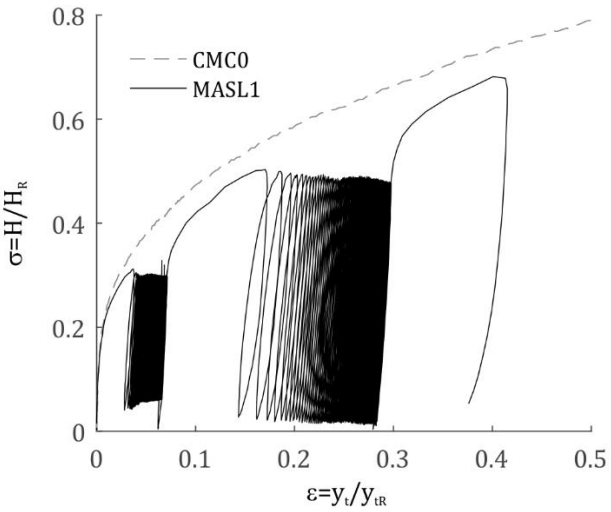

Figure 5: Test MASL1: Load-deflection curve

using different testing equipment (1-g and centrifuge) (e.g. Peralta, 2010, Klinkvort, 2012).

2.5 Multi-amplitude cyclic loading

The effect of cyclic loading on capacity is explored through a series of cyclic loading tests of the same load magnitude but different cycle number, immediately followed by a monotonic reloading (CMC0-5, CMLT2, Figure 4). For clarity, the past cyclic load history is not plotted on the graph but is indicated by the dashed line at maximum peak load. Each reloading curve is plotted from the final cyclic deformation to put each into context. The graph shows that, despite the effects of ratcheting, on exceeding the maximum cyclic load, the curve tends to rejoin the initial backbone curve. This conforms to the second observation made by Pyke (1979).

Finally, a series of cyclic load packets at different magnitudes was applied, with a typical load-deflection response displayed in Figure 5. The standard backbone curve is also plotted. The results conform to the above, showing that the key features characterising the pile response are:

(i) For each load packet, on initial reloading exceeding the maximum past cyclic load, the response tends towards re-joining the backbone curve. This means that the extended Masing rules still apply after cyclic loading.

(ii) However, this mechanism is competing with ratcheting, which moves the global response away from the backbone curve.

3. Constitutive modelling

3.1 Model description

The model described here is derived through the hyperplasticity framework, a novel approach for modelling plasticity behaviour that is more concise and rigorous than the standard methods widely used to date. The mathematical background of the approach is thoroughly described in Houlsby and Puzrin (2006) and full details of the model presented below are provided in Houlsby *et al.* (2017). For consistency, the notation adopted here are the same as in Houlsby *et al.* (2017). The model is expressed in terms of stress (σ) and strain (ε), for application to the experimental results through Equations 1 and 2.

The model provides a 0-D representation of the soil-pile macro-response outlined experimentally, which could be used in a structural analysis of a wind turbine. This justifies the consideration of H and y at the location of load application as this bypasses the need for a two-variable model to capture both rotation and displacement at ground level.

Masing (1926) and Pyke (1979) showed that models employing pure kinematic hardening give rise to the extended Masing rules. Hence, the starting point of the model developed below is kinematic hardening. A typical multi-surface kinematic hardening model is described using the schematic representation of Figure 6(a) (Houlsby and Puzrin, 2006). On loading the system, the springs (H_n) of each individual unit contribute to the global response when the corresponding slider reaches the threshold value (k_n). The typical response is shown in Figure 6(b). A choice of a large number of spring-slider units, or yield surfaces N_S, enables computation of a smooth continuous curve (Figure 6(c)). For a load-controlled case, the incremental strain response would be defined according to:

$$d\varepsilon = \frac{d\sigma}{E} + \sum_{n=1}^{N} d\alpha_n \qquad (7)$$

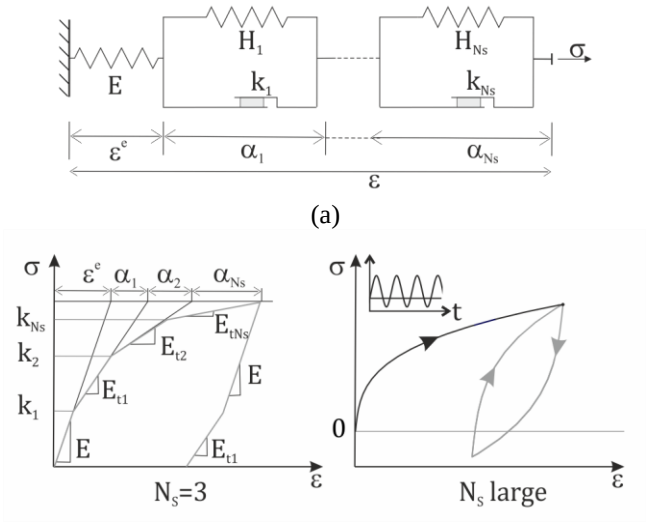

Figure 6: Kinematic hardening model: (a) schematic representation, (b, c) incremental response

where the incremental plastic strains are defined according to the family of yield surfaces:

$$\forall n \in [1, N_S] \quad |\sigma - H_n \alpha_n| \leq k_n \tag{8}$$

As illustrated in Figure 6(c), this model provides a stabilised loop when predicting cyclic loading. This is the case of most standard models and further development is required to implement the second key feature of the monopile response: ratcheting.

Using this base model, a new ratcheting element is added (Figure 7(a)). This creates an additional increment of strain $d\alpha_r$ for each increment of plastic strain, in the direction of loading:

$$d\alpha_r = S(\sigma) \sum_{n=1}^{N} R_n |d\alpha_n| \tag{9}$$

The amount of ratcheting strain generated by each hardening surface is characterised by the ratcheting rate R_n within that surface and now:

$$d\varepsilon = \frac{d\sigma}{E} + \sum_{n=1}^{N} d\alpha_n + d\alpha_r \tag{10}$$

with the increment of plastic strain still defined by Equation 6. This modified model, called HARM, provides the incremental response of Figure 7(b), featuring both key mechanisms of Section 2.5.

3.2 Computation of large number of cycles

To model large cycle numbers (typically for monopiles, above 10^8 cycles), incremental calculations such as the above are computationally prohibitive. However, because of the definition of the ratcheting strain, it is possible to accelerate the effects of ratcheting by multiplying the rate R_n by a factor R_{fac} corresponding to the number of cycles

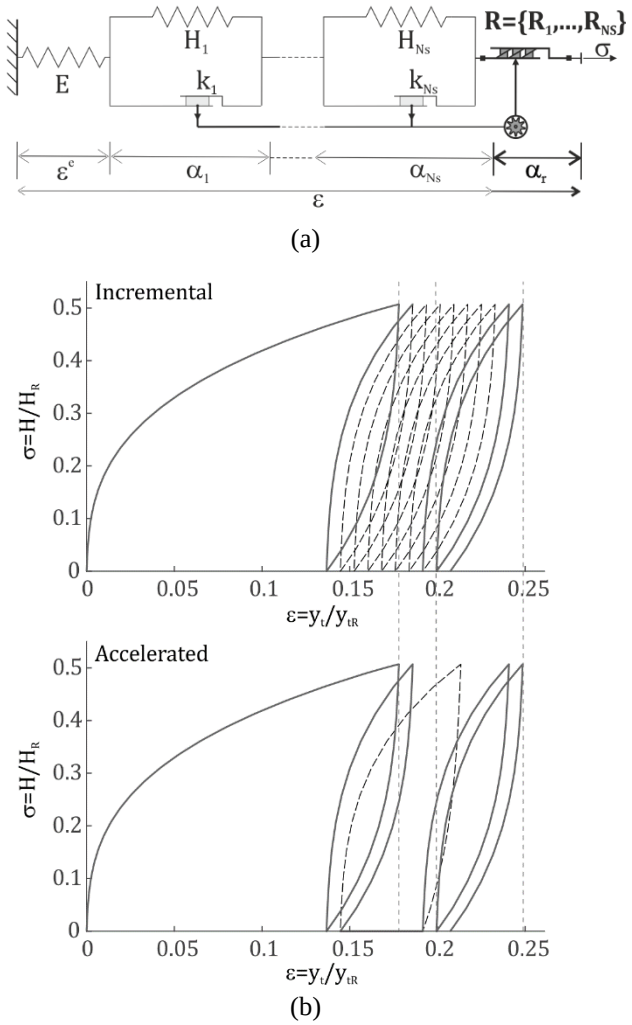

Figure 7: Typical kinematic hardening and ratcheting model: (a) schematic representation, (b) typical incremental and accelerated response

Table 2: Accelerated programme of Figure 7(b)

Incremental		Accelerated	
No. of Cycles	R_{fac}	No. of Cycles	R_{fac}
2	1	2	1
6	1	1	6
2	1	2	1

that are accelerated through. This is illustrated in Figure 7(b), where the programme of Table 2 was used. This is a powerful feature of the model, which is demonstrated on small numbers of cycles for clarity, but can be extended to a larger number of cycles (see later Table 3).

4. Application to Test Results

4.1 Kinematic hardening variables: backbone curve

The values for the stiffness H_n and strength k_n are calibrated in order to fit the kinematic hardening model to the desired shape of the backbone curve. For a range of model tests, a close fit is achieved with (Abadie, 2015):

$$\varepsilon = \sigma / E + \varepsilon_{pU} \left(\frac{\sigma}{k_U} \right)^{m_h} \tag{11}$$

Where ε_{pU}, m_h, E and k_U are found by direct fitting of the backbone curve. For test CMC0, this gives: ε_{pU}=1, m_h=3, E=84 and k_U= 1. Based on Equation 11, it can be shown that (Houlsby *et al.*, 2017):

$$k_n = k_U \frac{n-1}{N_S - 1}, n = 1 \ldots N_S \tag{12}$$

$$\begin{cases} H_1 = \dfrac{k_{Uo}}{\varepsilon_{pU}} \left(N_S - 1\right)^{m_h - 1} \\ H_{2 \le n < N_S} = \dfrac{H_1}{n^{m_h} - 2\left(n-1\right)^{m_h} + \left(n-2\right)^{m_h}} \\ H_{N_S} = 0 \end{cases} \tag{13}$$

This provides the kinematic hardening values.

4.2 Ratcheting behaviour

The ratcheting behaviour is specified by the rate of ratcheting, R_n. First, the amount of ratcheting deformation decreases with cycle number, which means that the ratcheting rate (R_n) decreases with cyclic load history. The implications of the above are twofold: (a) an additional variable that records the cyclic history is needed and (b) R_n will be a decreasing function of this new variable. The accumulated ratcheting strain β is hence defined:

$$d\beta = \left| d\alpha_r \right| \quad \Rightarrow \quad \beta = \sum_{increments} \left| d\alpha_r \right| \tag{14}$$

The choice of function for R_n is based on the experimental results of LeBlanc *et al.* (2010b) and Abadie (2015). They showed that, for the pile geometry and soil conditions explored, and in the case of 1-way cyclic loading, the accumulated deformation can be described by:

$$\begin{aligned} \beta_{pN} - \beta_{p0} &= \varepsilon_{pN} - \varepsilon_{p0} \\ &= T_0 {\zeta_b}^{m_\sigma} N^{m_\alpha} = T_0 {\sigma_{\max}}^{m_\sigma} N^{m_\alpha} \end{aligned} \tag{15}$$

with subscript p for the peak cyclic load. Because there is no displacement created by kinematic hardening (Masing rule), the accumulated deformation (ε_{pN}-ε_{p0}) is entirely due to ratcheting (β_{pN}-β_{p0}). m_σ and m_α are empirical exponents found to be equal to m_σ=4 and m_α=0.31 and T_0 is a dimensionless parameter of 0.5 (Abadie, 2015).

According to the above equation, it is expected that the rate of ratcheting will also depend on the stress level. For both cases, a power law function is chosen so that R_n is expressed as:

$$R_n = R_0 \left(\frac{k_n}{\sigma_0} \right) \left(\frac{\beta}{\beta_0} \right)^{-m_r} \left(\frac{|\sigma|}{\sigma_0} \right)^{m_s} \tag{16}$$

R_0 is the initial rate of ratcheting and m_r and m_s are empirical exponents. σ_0 is the ultimate stress level, which by definition of σ, is equal to 1. β_0 is the initial value of hardening strain, which is an arbitrarily small value compared with β_{p0}, introduced for normalisation purposes. The term $\left(k_n / \sigma_0\right)$ enables to adapt the ratcheting rate to each hardening surface.

Finally, the equation of any unload-reload loop provides an analytical expression for the ratcheting strain at peak load β_{pN}:

$$\beta_{pN}^{m_r+1} = \beta_0^{m_r+1} + R_\beta \varepsilon_{pU} \kappa_{m0} \left(1 + \kappa_m N\right) \left(\frac{\sigma_{\max}}{k_U} \right)^{m_s + m_h + 1} \tag{17}$$

$$\kappa_{m0} = \frac{\left(m_h - 1\right)\left(m_r + 1\right)}{m_s + m_h + 1} \tag{18}$$

$$\kappa_m = \frac{1}{2^{m_h}} \left(\left(m_s + m_h + 1\right) B\left(m_s + 1, m_h + 1\right) + 1 \right) \tag{19}$$

Where $B(x,y)$ is the beta function and $R_\beta = R_0 {\beta_0}^{m_r}$. A reasonable fit to the experimental data CMLT1-3 is obtained with m_r=3, m_s=12 and R_β=0.8.

4.3 Comparison with experimental results

The calibrated model is used to simulate the tests described in Table 1. Figure 8 shows the predicted response of test HIM, demonstrating that the model captures the Masing behaviour and that ratcheting deformation is negligible during a perfectly symmetric load reversal.

Figure 9(a) displays the stress-strain curve obtained for test CMLT3, computed using the accelerated programme of Table 3. The results exhibit the key features outlined in Section 2 and the graph compares favourably with that of Figure 3.

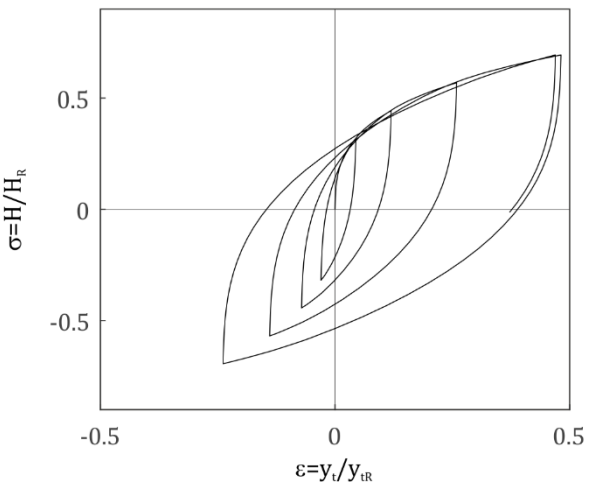

Figure 8: Predicted response for test HIM

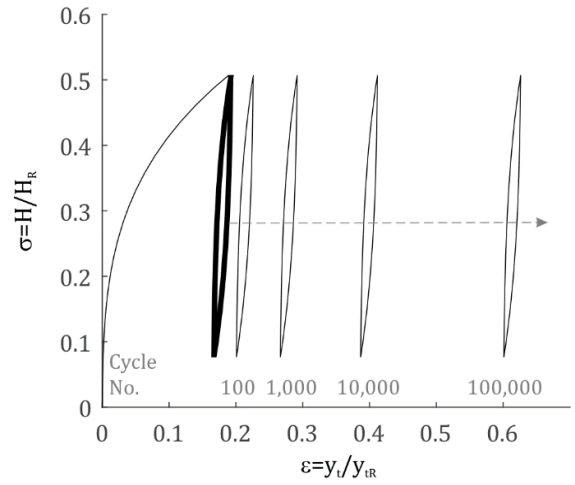

(a)

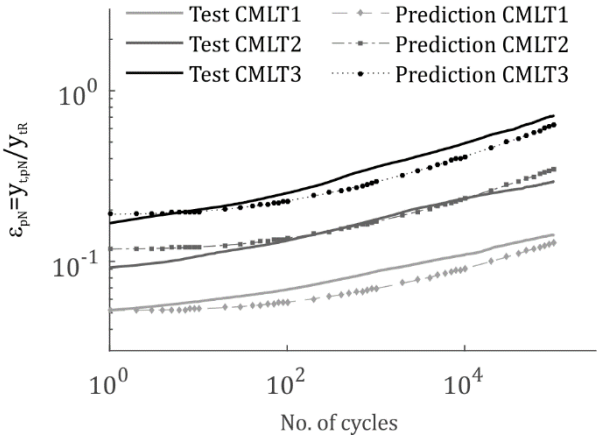

(b)

Figure 9: Continuous cyclic tests: (a) Predicted load-deflection curve (CMLT3), (b) Measured and predicted deflection at peak strain (CMLT1-3)

Table 3: Accelerated programme, tests CMLT1-3, Figure 9

Incremental		**Accelerated**	
No. of Cycles	R_{fac}	No. of Cycles	R_{fac}
10	1	10	1
90	1	9	10
1	1	1	1
900	1	9	100
1	1	1	1
9000	1	9	1000
1	1	1	1
90000	1	9	10000
1	1	1	1
100,000 cycles computed		50 cycles computed	

Figure 9(b) compares the measured and predicted evolution of the deformation at peak load with cycle number, for tests CMLT1-3. The graph demonstrates that the model predicts the experimental tests well, capturing both the evolution with cycle number and the effect of the load magnitude accurately.

The model is applied to the multi-amplitude cyclic load cases of Table 1. First, tests CMC0-5 and CMLT2 were simulated and the re-load curves are shown in Figure 10. Comparison with Figure 4 shows good agreement with the experimental trends. Likewise, the predicted response of test MALL3

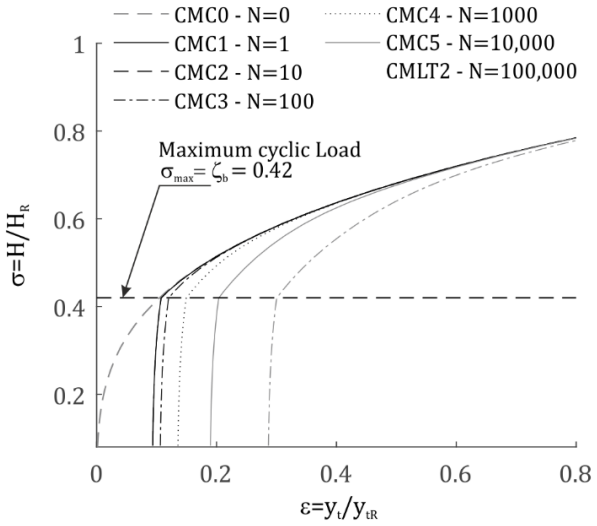

Figure 10: Predicted monotonic re-loading response, tests CMC0-5+CMLT2

displayed in Figure 11 shows that the resulting stress-strain curve represents the experimental response fairly well (Figure 5). In both cases, the responses feature a competition between (i) Masing behaviour and (ii) ratcheting; this is the key modelling objective of HARM.

Finally, Figure 11(b) shows the evolution of predicted and measured displacement at peak load, for tests MALL1-3. The results demonstrate that the trends are properly captured, while the quantitative values over-predict the final deformation.

5. Conclusions

This paper outlines a new modelling approach for rigid monopiles subjected to lateral cyclic loading. The methodology builds on experimental test results, identifying that the key mechanisms driving the pile response are a competition between (i) Masing behaviour and (ii) accumulated ratcheting deformation with cycle number.

These results underpin the development of a constitutive model, HARM. A methodology for calibration has also been highlighted and the predicted responses demonstrate close match with experimental results, with an accurate prediction of the key mechanisms that were initially identified.
Since the complete load-deflection response of any unload-reload loop is captured, the change in stiffness and damping can also be predicted. This point is not developed further here but is explored in more detail through Abadie (2015).

This paper provides the basis for a more extensive study, aimed at providing rigorous theoretical models, properly calibrated against experimental data, to be used with confidence by industry for

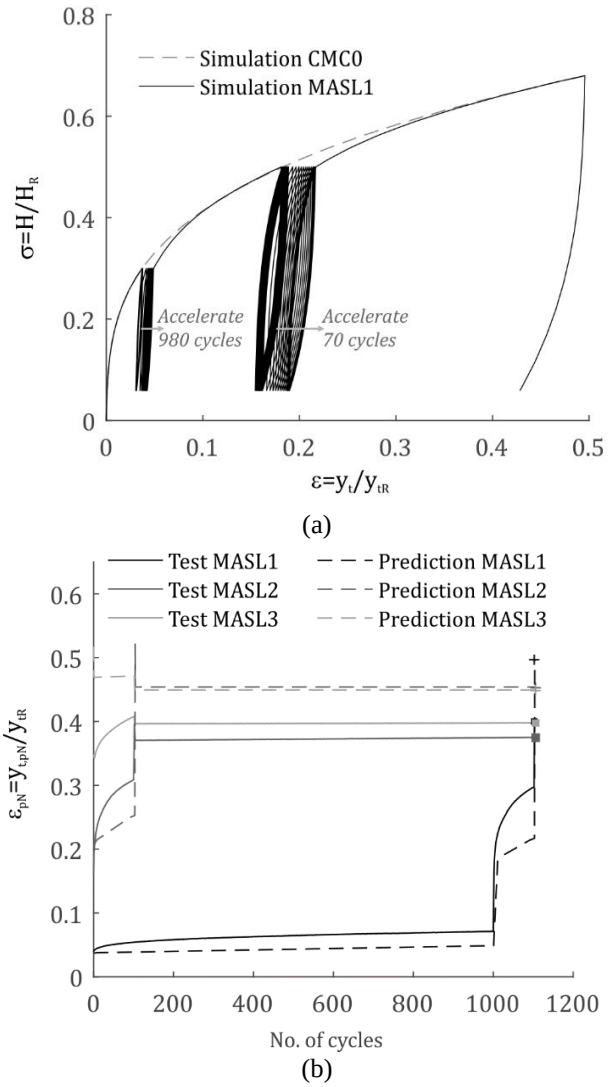

Figure 11: Multi-amplitude cyclic tests: (a) Predicted load-deflection curve (Test MASL1), (b) Measured and predicted deflection at peak strain (Tests MASL1-3)

design of the next generation of offshore foundations. On-going and future research explores extension of this modelling concept to Winkler-type approaches and 3D Finite Element Analyses, as well as more complex soil and loading conditions (*e.g.* multi-directional, partially-drained to undrained sands and clays, layered soils).

Acknowledgements

We are grateful to EDF Energies Nouvelles and EDF R&D as well as more recently DONG Energy for their funding of this work, including the financial support of the first Author.

References

Abadie, C. N. (2015) Cyclic Lateral Loading of Monopile Foundations in Cohesionless Soils. DPhil Thesis, Univ. of Oxford.

Abadie, C. N. & Byrne, B. W. (2014) Cyclic loading response of monopile foundations in cohesionless soils. *8th Int. Conf. on Physical Modelling in Geotechnics.* Perth, Australia.

Abadie, C. N., Byrne, B. W. & Houlsby, G. T. (2017) Cyclic plastic response of stiff piles in sand. Submitted to Géotechnique.

API (2010) Recommended Practice for Planning, Designing and Constructing Fixed Offshore Platforms, RP2A-WSD.

Byrne, B. W. *et al.* (2015) New design methods for large diameter piles under lateral loading for offshore wind applications. *Proc. of the 3rd Intern. Symposium on Frontiers in Offshore Geotechnics (ISFOG).* Oslo, Norway.

DNV (2014) Offshore Standard DNV-OS-J101, Design of offshore wind turbine structures.

Houlsby, G. T., Abadie, C. N., Beuckelaers, W. J. A. P. & Byrne, B. W. (2017) A model for nonlinear hysteretic and ratcheting behaviour. *Intern. Journal of Solids and Structures*, In Press.

Houlsby, G. T. & Puzrin, A. M. (2006) *Principles of Hyperplasticity: an Approach to Plasticity Theory Based on Thermodynamic Principles,* London.

Kallehave, D., LeBlanc-Thilsted, C. & Liingaard, M. A. (2012) Modification of the API formulation of initial stiffness of sand. *Proc. of the 7th Intern. Conf. on Offshore Site Investigation and Geotechnics (OSIG).* London, UK.

Klinkvort, R. T. (2012) Centrifuge modelling of drained lateral pile-soil response. PhD Thesis, DTU.

LeBlanc, C., Byrne, B. W. & Houlsby, G. T. (2010a) Response of Stiff Piles to Random Two-Way Lateral Loading. *Géotechnique,* 60**,** 715-721.

LeBlanc, C., Houlsby, G. T. & Byrne, B. W. (2010b) Response of Stiff Piles in Sand to Long-term Cyclic Lateral Loading. *Géotechnique*, 60**,** 79-90

Masing, G. (1926) Eiganspannungen und Verfestigung beim Messing. *Proceedings for the 2nd Intern. Congress of Applied Mechanics.*

Miner, A. M. (1945) Cumulative damage in fatigue. *Journal of applied mechanics***,** 12, 159-165.

O'Neill, M. W. & Murchison, J. M. (1983) An evaluation of p-y relationships in cohesionless soils. (Ed., Dep. of Civil Engineering, Univ. of Houston, Texas.

Peralta, P. (2010) Investigations on the Behavior of Large Diameter Piles under Long-Term Lateral Cyclic Loading in Cohesionless Soil. PhD thesis, Univ. of Hannover.

Pyke, R. M. (1979) Nonlinear soil models for irregular cyclic loadings. *Journal Geotechnical Engineering Division, ASCE*, 105**,** 715-726.

Rovere, M. (2004) Cyclic loading test machine for caisson suction foundations. Centrale Lille and Politechnico di Milano.